Shift of the photoelectron momentum against the radiation pressure force in linearly polarized intense midinfrared laser fields

Rešad Kahvedžić [*]

Institute of Physical Chemistry, Friedrich Schiller University Jena, Helmholtzweg 4, 07743 Jena, Germany
and Max Planck School of Photonics, Hans-Knöll-Straße 1, 07745 Jena, Germany

Stefanie Gräfe [†]

Institute of Physical Chemistry, Friedrich Schiller University Jena, Helmholtzweg 4, 07743 Jena, Germany;
Max Planck School of Photonics, Hans-Knöll-Straße 1, 07745 Jena, Germany;
and Fraunhofer Institute for Applied Optics and Precision Engineering, Albert-Einstein-Straße 7, 07745 Jena, Germany

The propagation direction momentum component of direct photoelectrons emitted by ionization of an atomic target in an intense, linearly polarized, midinfrared laser field is analyzed. Within the dipole approximation, the average value of this component is zero. However, when nondipole corrections are included, it becomes nonzero. Applying the saddle-point approximation to compute the integral over the ionization times in the expression for the nondipole strong-field approximation differential ionization rate, we surprisingly find a negative momentum shift, corresponding to a shift against the radiation pressure force. Our analysis shows that there is a positive contribution originating from individual ionization pathways within one optical cycle. The interference of contributions from ionization pathways arising within the same optical cycle of the field (intracycle interference) causes an oscillatory behavior, which, crossing to negative values, induces the shift against the radiation pressure force.

I. INTRODUCTION

Transfer of momentum from the electromagnetic field to a target manifests itself through the radiation pressure force acting on the target. The force accelerates the target, propelling it in the propagation direction of the field [1]. Theoretically accounting for this effect requires treatment of the field beyond the dipole approximation, i.e., the spatial dependence of the field must be included.

In laser-induced ionization processes of atomic and molecular targets, the momentum transfer results in an asymmetric photoelectron momentum distribution (PMD) along the field propagation direction, as demonstrated by investigations presented in a number of recent works [2–36]. The total energy E_{tot} supplied by the laser field in ionization processes is related to the total momentum transferred to the target in the propagation direction by E_{tot}/c, where c is the speed of light. One part of the energy is used to liberate the electron from a bound state of energy $-I_P$ while the excess energy is carried away as the kinetic energy of the emitted electron $E_{\mathbf{p}}$. It was shown that the photoelectron carries away 1/3 of the momentum associated with the ionization potential I_P [$I_P/(3c)$] in the strong-field ionization regime [7,8,15]. Experiments confirmed this result for circularly polarized fields [27]. In the cases of intense linearly and elliptically polarized fields with small values of ellipticity, field-induced rescattering becomes important, and a shift of the momentum in the direction opposite to the radiation pressure force occurs. This counterintuitive shift was explained with the combined effect of Coulomb focusing and the magnetic field [11,12,27,37]. For more details, we refer the reader to one of the recent reviews [38–40].

In this work we investigate the propagation direction momentum component of direct photoelectrons emitted by ionization of an atomic target in an intense, linearly polarized, long midinfrared laser field. For this purpose, the nondipole strong-field approximation (SFA) introduced in our recent publication of Ref. [33] is applied. The approach is extended by utilizing the saddle-point approximation to evaluate the time integral appearing in the nondipole SFA differential ionization rate. For the linearly polarized long field we obtain analytic solutions of the saddle-point equation and perform an analytic computation of the partial average value of the propagation direction momentum component. We demonstrate that the contributions of individual saddle points give strictly positive values. However, the complete expression, including the interference of contributions from the saddle points originating in the same optical cycle (intracycle interference) leads to a shift against the radiation pressure force. We illustrate that, even when rescattering of emitted photoelectrons on their parent core is not included, a shift of the propagation direction momentum component against the radiation pressure force may occur and we trace its origin to the oscillatory behavior induced by the intracycle interference.

---
[*]resad.kahvedzic@uni-jena.de
[†]s.graefe@uni-jena.de

The article is structured in the following way. In Sec. II, we introduce the theoretical formalism, apply the saddle-point approximation and obtain the solutions of the saddle-point equation with nondipole corrections for the case of a linearly polarized long field. Moreover, the main result of the article is presented and discussed. Finally, the article is summarized in Sec. III. Unless otherwise stated, atomic units are used throughout the article.

II. THEORY AND DISCUSSION

A. Theoretical formalism

The nonrelativistic strong-field ionization beyond the dipole approximation is described as in Ref. [33]. Shortly, the SFA is extended beyond the dipole approximation by expanding the vector potential $\mathbf{A}(\mathbf{r}, t)$ in powers of $1/c$ and retaining terms up to the first order. This corresponds to replacing the dipole approximation vector potential $\mathbf{A}(t)$ by $\mathbf{A}(t) + \frac{\hat{\mathbf{k}} \cdot \mathbf{r}}{c} \mathbf{E}(t)$ ($\hat{\mathbf{k}}$ is the unit vector in the propagation direction) [41]. Correctly accounting for the terms that are of higher order in $1/c$ would require a relativistic treatment (see, e.g., Refs. [42,43]). The pulse propagates along the z axis, with the electric field polarized along the x axis $\mathbf{E}(t) = \mathbf{e}_x E_0 \cos(\omega t)$. E_0 is the amplitude of the field and ω is the frequency of the field with period $T = 2\pi/\omega$. The differential ionization rate upon absorption of n photons for the direct photoelectrons is [33]

$$w_{\mathbf{p}i}(n) = 2\pi p |T_{\mathbf{p}i}(n)|^2. \tag{1}$$

The integer n relates to the energy conservation

$$E_{\mathbf{p}} + I_P + U_P(1 + p_z/c) = n\omega, \tag{2}$$

where $E_{\mathbf{p}} = \mathbf{p}^2/2$ is the kinetic energy, I_P is the ionization potential and U_P is the ponderomotive energy, $U_P = A_0^2/4$. $T_{\mathbf{p}i}(n)$ is the T-matrix element for the transition from the initial (ground) state $|\psi_i\rangle \, e^{iI_P t}$ to the nondipole Volkov state $|\pi(\mathbf{p}, t)\rangle \, e^{-iS(\mathbf{p}, t)}$

$$T_{\mathbf{p}i}(n) = \int_0^T \frac{dt}{T} \langle \pi(\mathbf{p}, t) | H_{\text{int}}(t) | \psi_i \rangle \, e^{i\phi(t)}. \tag{3}$$

The time integration in Eq. (3) is performed over the ionization times within one period T of the long laser field. The modified canonical momentum with the nondipole correction in the square bracket is

$$\pi(\mathbf{p}, t) = \mathbf{p} + \mathbf{A}(t) + [\mathbf{p} \cdot \mathbf{A}(t) + \mathbf{A}^2(t)/2]\mathbf{e}_z/c, \tag{4}$$

and the phase is $\phi(t) = S(\mathbf{p}, t) + I_P t$. The nondipole Volkov phase up to the first order in $1/c$ reads

$$S(\mathbf{p}, t) = \frac{1}{2} \int^t dt' \pi^2(\mathbf{p}, t')$$
$$= E_{\mathbf{p}} t + [\mathbf{p} \cdot \boldsymbol{\alpha}(t) + U_P t + U_1(t)][1 + p_z/c]. \tag{5}$$

The vector potential is

$$\mathbf{A}(t) = -\int^t dt' \mathbf{E}(t') = -\mathbf{e}_x A_0 \sin(\omega t), \tag{6}$$

with the amplitude $A_0 = E_0/\omega$. The remaining quantities are

$$\boldsymbol{\alpha}(t) = \int^t dt' \mathbf{A}(t') = \mathbf{e}_x A_0 \cos(\omega t)/\omega \tag{7}$$

and

$$U_1 = \int^t dt' \mathbf{A}(t')^2/2 - U_P t = -A_0^2 \sin(2\omega t)/(8\omega). \tag{8}$$

The dependence of the T-matrix element, Eq. (3), on the integer n is reflected through the energy conservation imposed by Eq. (2). The interaction Hamiltonian is given by

$$H_{\text{int}}(t) = \left(\mathbf{r} - i\frac{z}{c}\nabla \right) \cdot \mathbf{E}(t). \tag{9}$$

B. Saddle-point approximation

To solve the integral in Eq. (3), we apply the saddle-point approximation [44], which leads to the result

$$T_{\mathbf{p}i} \approx \frac{1}{T} \sum_{t_s} \sqrt{\frac{2\pi i}{\phi''(t_s)}} \langle \pi(\mathbf{p}, t_s) | H_{\text{int}}(t_s) | \psi_i \rangle \, e^{i\phi(t_s)}. \tag{10}$$

The summation is performed over the saddle-point times t_s. They are obtained as the solutions of the saddle-point equation

$$\partial_t \phi(t)|_{t=t_s} = \pi^2(\mathbf{p}, t_s)/2 + I_P = 0. \tag{11}$$

Equation (11) yields complex saddle-point times which are interpreted as ionization times. Their complexity relates to the quantum tunneling nature of ionization [45]. Each saddle-point time t_s corresponds to a different ionization pathway [46]. The second derivative of the phase at t_s, up to $1/c$, is

$$\phi''(t_s) = -\mathbf{E}(t_s) \cdot [\mathbf{p} + \mathbf{A}(t_s)][1 + p_z/c]. \tag{12}$$

With the above expressions for the field-related quantities entering $\pi(\mathbf{p}, t_s)$, Eq.(4), the saddle-point equation, Eq. (11), reduces to

$$\left[\sin^2(\omega t_s) - 2\frac{p_x}{A_0}\sin(\omega t_s) \right]\left[1 + \frac{p_z}{c} \right] + \frac{E_{\mathbf{p}} + I_P}{2U_P} = 0, \tag{13}$$

where terms of the second order in $1/c$ are neglected. Physically meaningful solutions satisfy

$$0 \leqslant \omega t_s^R < 2\pi, \quad \omega t_s^I > 0, \tag{14}$$

with $t_s^R = \text{Re}(t_s)$ and $t_s^I = \text{Im}(t_s)$. The first requirement assures that only ionization times within one optical cycle contribute to the T-matrix element in Eq. (3). The second requirement guarantees the convergence of the integral solved by applying the saddle-point approximation to obtain Eq. (10). The quadratic equation in $\sin(\omega t_s)$, Eq. (13), is solved by

$$\sin(\omega t_s)_\pm = \frac{p_x}{A_0} \pm i\sqrt{\frac{E_{\mathbf{p}} + I_P}{2U_P\left(1 + \frac{p_z}{c}\right)} - \left(\frac{p_x}{A_0}\right)^2} = z_\pm. \tag{15}$$
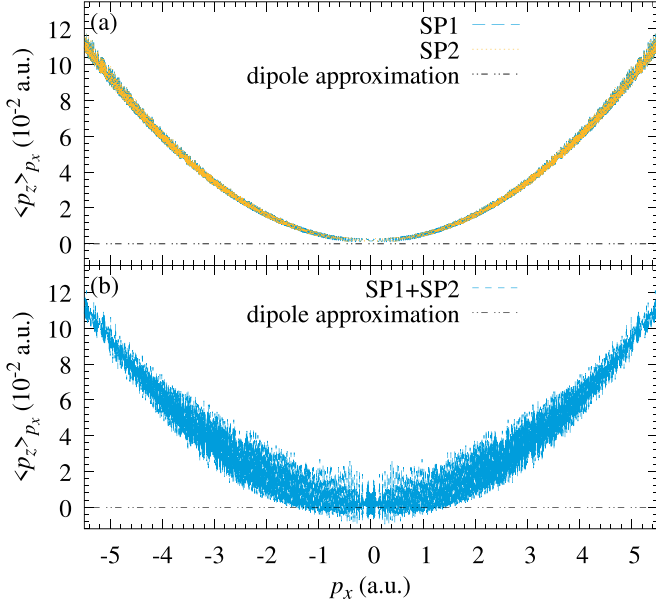
FIG. 1. The partial average of p_z as a function of p_x, Eq. (18), for the 1s initial state of the hydrogen atom. The field intensity is $I = 1.4 \times 10^{14}$ W/cm^2 and the wavelength is $\lambda = 4$ μm. (a) the individual contributions from saddle points t_{s1} (SP1) and t_{s2} (SP2). (b) The coherent sum of the contributions from the two saddle points. The dipole approximation result is obtained by setting $1/c = 0$.

There are two solutions satisfying Eq. (14). For $p_x \geqslant 0$, the corresponding complex inverse sines can be expressed as

$$\omega t_{s1} = -i\mathrm{Ln}\left(iz_+ + \sqrt{1 - z_+^2}\right),$$

$$\omega t_{s2} = -i\mathrm{Ln}\left(iz_- - \sqrt{1 - z_-^2}\right). \quad (16)$$

Real parts ωt_{s1}^R and ωt_{s2}^R appear in the falling and rising edge of $\mathbf{E}(t)$ symmetrically around $\pi/2$ while for the imaginary parts $\omega t_{s1}^I = \omega t_{s2}^I$ holds. For $p_x < 0$, Eq. (14) is satisfied by

$$\omega t_{s1} = -i\mathrm{Ln}\left(iz_- - \sqrt{1 - z_-^2}\right) + 2\pi,$$

$$\omega t_{s2} = -i\mathrm{Ln}\left(iz_+ + \sqrt{1 - z_+^2}\right) + 2\pi, \quad (17)$$

so that real parts ωt_{s1}^R and ωt_{s2}^R appear symmetrically around $3\pi/2$ and the imaginary parts remain the same as for $p_x \geqslant 0$. The above equations refer to the principal values of the complex logarithm and the square root.

C. Discussion

We investigate the partial average

$$\langle p_z \rangle_{p_x} = \frac{\int dp_y dp_z \, p_z w_{\mathbf{p}i}}{\int dp_y dp_z \, w_{\mathbf{p}i}}. \quad (18)$$

To evaluate it, we compute the three-dimensional (3D) PMD via Eqs. (17), (16), (10), and (1) and numerically solve the integrals over p_y and p_z. In Fig. 1, we present the results for the hydrogen atom, with the 1s initial wave function given by $\psi_i(r) = e^{-r}/\sqrt{\pi}$ and the ionization potential
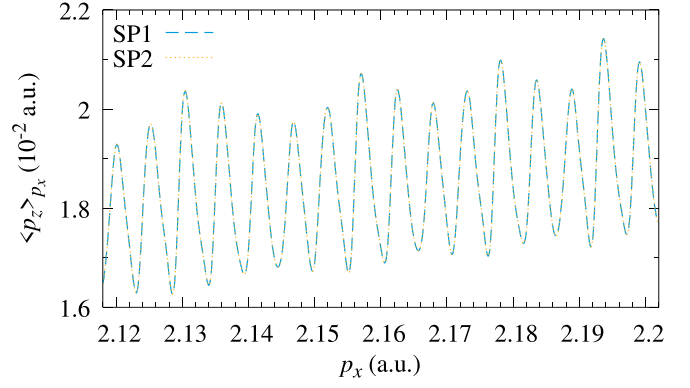
FIG. 2. Part of Fig. 1(a) for $p_x \in [2.118, 2.202]$ a.u.

$I_P = 0.5$ a.u. (13.605 eV). The corresponding interaction matrix element for a generic momentum $\mathbf{q}$ is (see Ref. [33])

$$\langle \mathbf{q}|H_{\mathrm{int}}(t)|\psi_i \rangle = -i\frac{8\sqrt{2}}{\pi} \frac{\mathbf{q} \cdot \mathbf{E}(t)}{(\mathbf{q}^2 + 1)^3}\left(1 + \frac{q_z}{c}\right). \quad (19)$$

The applied field intensity is $I = 1.4 \times 10^{14}$ W/cm^2 and the wavelength is $\lambda = 4$ μm. Figure 1(a) displays the results obtained for two individual saddle-point times t_{s1} (SP1) and t_{s2} (SP2) in Eq. (10). The two saddle points separately yield the same figure for $\langle p_z \rangle_{p_x}$, which, as we show below, closely oscillates around the parabola $p_x^2/(2c) + I_P/(3c)$ with strictly positive values. The positive values of $\langle p_z \rangle_{p_x}$ imply a forward shift of the PMD along the field propagation direction (in the direction of the radiation pressure force). The sum of the contributions from the two saddle points t_{s1} and t_{s2} [SP1 + SP2 in Fig. 2(b)] in Eq. (10) yields a result which features rapid oscillations with a larger amplitude around a similar parabolic figure. These oscillations, caused by the intracycle interference of contributions from the two saddle points, cross to negative values for smaller values of p_x, implying a backward shift of the PMD along the field propagation direction, i.e., a shift against the radiation pressure force. We note that this is a purely nondipole effect. Within the dipole approximation, $\langle p_z \rangle_{p_x}$ is zero everywhere because the corresponding PMD is symmetric along the propagation direction.

The oscillations present in Fig. 1(a) are, on the contrary, the consequence of the intercycle interference, i.e., the interference of contributions originating from different cycles of the field, which lead to the same final momentum. The intercycle interference pattern in energy spectra consists of equidistant peaks separated by the photon energy ω [47]. As a consequence of the periodicity of the long field that we here use, the contributions from different cycles are compressed in the energy conservation Eq. (2), see, e.g., Ref. [48] and references therein. To demonstrate this, we consider Eq. (2) for an integer n. As we are interested in $\langle p_z \rangle_{p_x}$ as a function of p_x, we set $p_y = 0$. Furthermore, p_z behaves as the already mentioned parabola $p_x^2/(2c) + I_P/(3c)$ in Fig. 1(a) and, because the kinetic energy is quadratic in momentum, gives a contribution of the order $O(1/c^2)$ to the kinetic energy, which we neglect. As a result, we have the equation $(p_x^{(n)})^2/2 + I_P + U_P = n\omega$. Considering two neighboring values, n and $n + 1$, we obtain the relation $p_x^{(n+1)} = \sqrt{2\omega + (p_x^{(n)})^2}$ that connects two

TABLE I. Approximate locations of the peaks in Fig. 2 computed as explained in the main text.

Peak	p_x (a.u)	Peak	p_x (a.u.)
1	2.120	9	2.163
2	2.125	10	2.168
3	2.131	11	2.173
4	2.136	12	2.178
5	2.141	13	2.184
6	2.147	14	2.189
7	2.152	15	2.194
8	2.157	16	2.199

neighboring peaks along the p_x direction. Figure 2 shows a zoomed-in part of Fig. 1(a) for $p_x \in [2.118, 2.202]$ a.u.. The first peak in Fig. 2 is located at $p_x^{(1)} \approx 2.120$ a.u.. We can now compute $p_x^{(2)} = \sqrt{2\omega + (p_x^{(1)})^2} \approx 2.125$ a.u., which gives us the position of the second peak. Continuing this iteration for the range of p_x in Fig. 2, we obtain the values presented in Table I. It predicts that, for the considered range of p_x, there are 16 peaks and gives their positions along the p_x direction, which agrees with Fig. 2.

To analyze the shift against the radiation pressure force in more detail, we restrict the problem to the p_x-p_z plane ($p_y = 0$). This simplification allows us to approximate Eq. (18) with simple, analytically solvable integrals. The complete expression for the phase $\phi(t)$ is

$$
\phi(t) = \left[E_{\mathbf{p}} + I_P + U_P\left(1 + \frac{p_z}{c}\right) \right] t
$$
$$
+ \left[\frac{p_x A_0}{\omega} \cos(\omega t) - \frac{A_0^2}{8\omega} \sin(2\omega t) \right] \left[1 + \frac{p_z}{c} \right]. \quad (20)
$$

Extracting the real $\{\phi_s^R = \text{Re}[\phi(t_s)]\}$ and imaginary $\{\phi_s^I = \text{Im}[\phi(t_s)]\}$ parts of the phase at the saddle-point times leads to

$$
\phi_s^R = \left[E_{\mathbf{p}} + I_P + U_P\left(1 + \frac{p_z}{c}\right) \right] t_s^R
$$
$$
+ \left[\frac{p_x A_0}{\omega} \cos(\omega t_s^R) \cosh(\omega t_s^I) \right.
$$
$$
\left. - \frac{A_0^2}{8\omega} \sin(2\omega t_s^R) \cosh(2\omega t_s^I) \right] \left[1 + \frac{p_z}{c} \right], \quad (21)
$$

$$
\phi_s^I = \left[E_{\mathbf{p}} + I_P + U_P\left(1 + \frac{p_z}{c}\right) \right] t_s^I
$$
$$
- \left[\frac{p_x A_0}{\omega} \sin(\omega t_s^R) \sinh(\omega t_s^I) \right.
$$
$$
\left. + \frac{A_0^2}{8\omega} \cos(2\omega t_s^R) \sinh(2\omega t_s^I) \right] \left[1 + \frac{p_z}{c} \right]. \quad (22)
$$

Neglecting the prefactors containing the slowly varying interaction matrix element in Eqs. (1) and (10), we approximate the differential ionization rate as the sum of the contributions

from the phase ϕ at the two saddle-point times

$$
w_{\mathbf{p}i} \sim \left| e^{i\phi(t_{s1})} + e^{i\phi(t_{s2})} \right|^2 = \left| e^{i\phi_{s1}^R - \phi_{s1}^I} + e^{i\phi_{s2}^R - \phi_{s2}^I} \right|^2
$$
$$
= e^{-2\phi_{s1}^I} + e^{-2\phi_{s2}^I} + 2e^{-\phi_{s1}^I - \phi_{s2}^I} \cos\left(\phi_{s2}^R - \phi_{s1}^R\right). \quad (23)
$$

The first two terms represent the contributions from the individual saddle points which are exponentially decaying with the respective imaginary parts of the phases, whereas the third term accounts for their interference, oscillating with the difference of the real parts of the phases and exponentially decaying with the sum of the imaginary parts of the phases. Extracting the real and imaginary parts from Eq. (15) yields a nonlinear system of equations for t_s^R and t_s^I

$$
\sin\left(\omega t_s^R\right) \cosh\left(\omega t_s^I\right) = \frac{p_x}{A_0},
$$
$$
\cos\left(\omega t_s^R\right) \sinh\left(\omega t_s^I\right) = \pm\sqrt{\frac{E_{\mathbf{p}} + I_P}{2U_P\left(1 + \frac{p_z}{c}\right)} - \left(\frac{p_x}{A_0}\right)^2}. \quad (24)
$$

The small values of the imaginary component of the saddle-point times ($\omega t_s^I \ll 1$) justify keeping only the leading terms in the expansion of hyperbolic sine and hyperbolic cosine

$$
\sin\left(\omega t_s^R\right) \approx \frac{p_x}{A_0},
$$
$$
\cos\left(\omega t_s^R\right)\omega t_s^I \approx \pm\sqrt{\frac{E_{\mathbf{p}} + I_P}{2U_P\left(1 + \frac{p_z}{c}\right)} - \left(\frac{p_x}{A_0}\right)^2}. \quad (25)
$$

Expansion of the square root up to the second order in p_z in the above equation leads to the solutions in accordance with Eq. (14) for $p_x \geqslant 0$

$$
\omega t_{s1}^R \approx \arcsin\left(\frac{p_x}{A_0}\right),
$$
$$
\omega t_{s2}^R \approx \pi - \arcsin\left(\frac{p_x}{A_0}\right), \quad (26)
$$
$$
\omega t_s^I \approx \sqrt{\frac{2I_P}{A_0^2 - p_x^2}} \left[1 + \frac{p_z}{c} \frac{p_x^2 + 2I_P}{4I_P} + \frac{p_z^2}{4I_P} \right].
$$

Since $\omega t_{s1}^I = \omega t_{s2}^I$, we label the corresponding solution with ωt_s^I. For $p_x < 0$, the solutions are

$$
\omega t_{s1}^R \approx \pi + \arcsin\left(\frac{|p_x|}{A_0}\right),
$$
$$
\omega t_{s2}^R \approx 2\pi - \arcsin\left(\frac{|p_x|}{A_0}\right), \quad (27)
$$

where ωt_s^I is the same as in Eq. (26). From Eqs. (27), (26), and (22), it is clear that $\phi_{s1}^I = \phi_{s2}^I$, which we simply label with ϕ_s^I in the following. The imaginary part of the phase can now be approximated with the following expression [see Eqs. (27),
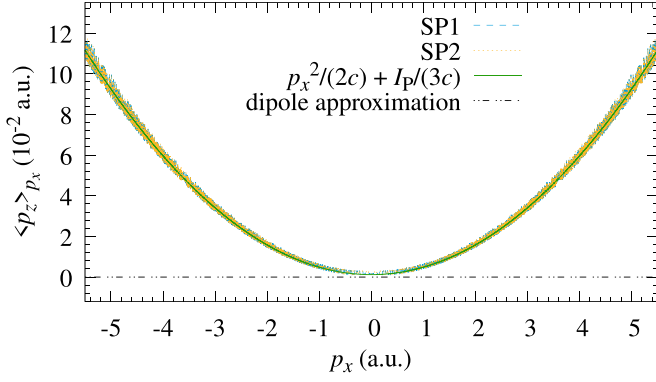
FIG. 3. Contributions from the individual saddle points SP1 and SP2 from Fig. 1(a) and the value represented by Eq. (34).

FIG. 4. The analytic estimate given by Eq. (33) and the value represented by Eq. (34).

(26), and (22)]:

$$
\phi_s^I \approx \frac{1}{\omega}\sqrt{\frac{2I_P}{A_0^2 - p_x^2}}\left[\frac{3}{4}p_z^2 - \frac{p_z}{c}\frac{3p_x^2 + 2I_P}{4} + I_P\right]. \tag{28}
$$

On the other hand, the difference of the real parts of the phases $(\Delta\phi_s^R = \phi_{s2}^R - \phi_{s1}^R)$ for the full range of p_x can be expressed as [see Eqs. (27), (26), and (21)]

$$
\Delta\phi_s^R \approx \left[\frac{p_x^2 + p_z^2}{2} + I_P + U_P\left(1 + \frac{p_z}{c}\right)\right]\frac{2\arccos\left(\frac{|p_x|}{A_0}\right)}{\omega}
$$
$$
- \frac{3|p_x|}{2\omega}\sqrt{A_0^2 - p_x^2}\left(1 + \frac{p_z}{c}\right). \tag{29}
$$

The differential ionization rate, Eq. (23), is now

$$
w_{\mathbf{p}i} \sim e^{-2\phi_s^I} + e^{-2\phi_s^I}\cos\left(\Delta\phi_s^R\right)
$$
$$
= e^{-2\phi_s^I} + \frac{1}{2}e^{-(2\phi_s^I + i\Delta\phi_s^R)} + \frac{1}{2}e^{-(2\phi_s^I - i\Delta\phi_s^R)}, \tag{30}
$$

which allows us to compute the partial average

$$
\langle p_z\rangle_{p_x} \sim \frac{\int_{-\infty}^{\infty}dp_z\, p_z w_{\mathbf{p}i}}{\int_{-\infty}^{\infty}dp_z\, w_{\mathbf{p}i}}. \tag{31}
$$

The arguments of the exponential functions in Eq. (31) are quadratic in p_z

$$
2\phi_s^I = \alpha p_z^2 - \beta p_z + \gamma,
$$
$$
2\phi_s^I \pm i\Delta\phi_s^R = \alpha_\pm p_z^2 - \beta_\pm p_z + \gamma_\pm, \tag{32}
$$

with the coefficients α, β, γ, $\alpha_\pm$, $\beta_\pm$, and $\gamma_\pm$ given in the Appendix. The integrals in Eq. (31) are now readily solved. Neglecting the terms beyond $1/c$ leads to the approximate result

$$
\langle p_z\rangle_{p_x} \sim \frac{\beta}{2\alpha}\frac{1 + \mathrm{Re}\left[\left(\frac{\alpha}{\alpha_+}\right)^{3/2}\frac{\beta_+}{\beta}\exp(\gamma - \gamma_+)\right]}{1 + \mathrm{Re}\left[\left(\frac{\alpha}{\alpha_+}\right)^{1/2}\exp(\gamma - \gamma_+)\right]}. \tag{33}
$$

The factor

$$
\frac{\beta}{2\alpha} = \frac{p_x^2}{2c} + \frac{I_P}{3c} \tag{34}
$$

is the result of contributions from individual saddle points, which is precisely the parabola found previously [7,8,27]. In contrast, the interference term gives a complicated function modifying it. The other factors present in Eq. (33) are given in the Appendix.

Figure 3 reveals the individual contributions from the two saddle points in Fig. 1(a) alongside the result of Eq. (34). It demonstrates that the always positive result obtained using the separate saddle points closely oscillates around the parabola given by $p_x^2/(2c) + I_P/(3c)$. The complete estimate, including the intracycle interference contribution, as given by Eq. (33), oscillates around the same parabola $p_x^2/(2c) + I_P/(3c)$ and for the range of $p_x \in [-1.4, 1.4]$a.u. takes negative values, see Fig. 4.

III. CONCLUSION

In conclusion, we employed the saddle-point approximation to solve the time integral in the nondipole SFA differential ionization rate expression. Two complex saddle points per optical cycle, corresponding to different ionization pathways, contribute. The two saddle points separately give the same result for the differential ionization rate but they feature different real parts of the ionization phase. Computing the partial average value of the propagation direction momentum component (p_z) as a function of the polarization direction momentum component (p_x), we demonstrated that individual ionization pathways lead to a forward momentum shift along the propagation direction, obeying the parabolic relation $p_x^2/(2c) + I_P/(3c)$. However, the intracycle interference, i.e., the interference of the ionization pathways from the two saddle-point solutions originating within the same optical cycle of the field, results in an oscillatory behavior around a parabola depending on the difference of the real parts of the ionization phases. Due to these oscillations, the momentum component can take negative values, suggesting a backward momentum shift along the propagation direction. As a nondipole effect studied with a nonrelativistic theoretical approach, this result is expected to be pronounced for light fields of high but nonrelativistic intensities and long

wavelengths starting from the midinfrared spectral region, where the motion of an electron along the field propagation direction becomes important, see, e.g., Ref. [49].

The present work does not consider the important effects of field-induced recollisions and Coulomb effects, which significantly affect the PMD in linearly polarized fields. Even when these effects to which the shift of the PMD against the radiation pressure force was previously attributed are not accounted for, we find that such a shift prevails. We here reveal that the mechanism causing the shift of momentum distributions of direct photoelectrons against the radiation pressure force originates in the intracycle interference of different ionization pathways leading to the same final momentum. The derivation leading to Eq. (33) accounts for the initial state only via the ionization potential I_P. This means that, in principle, any binding potential allowing for ionization from a bound state (e.g., the zero-range potential) would be characterized by the negative shift described here. We believe our result provides new insight into the discussion on the cause of this shift, as our approach does not incorporate recollisions and Coulomb focusing.

ACKNOWLEDGMENTS

APPENDIX

The coefficients in Eqs. (32)–(34) are

$$\alpha = \frac{3}{2\omega}\sqrt{\frac{2I_P}{A_0^2 - p_x^2}}, \tag{A1}$$

$$\beta = \frac{1}{2\omega c}\sqrt{\frac{2I_P}{A_0^2 - p_x^2}}\left(3p_x^2 + 2I_P\right), \tag{A2}$$

$$\gamma = \frac{(2I_P)^{3/2}}{\omega\sqrt{A_0^2 - p_x^2}}, \tag{A3}$$

$$\alpha_\pm = \alpha \pm i\frac{\arccos\left(\frac{|p_x|}{A_0}\right)}{\omega}, \tag{A4}$$

$$\beta_\pm = \beta \pm \frac{i}{c}\left[\frac{3|p_x|}{2\omega}\sqrt{A_0^2 - p_x^2} - \frac{2U_P\arccos\left(\frac{|p_x|}{A_0}\right)}{\omega}\right], \tag{A5}$$

$$\gamma_\pm = \gamma \pm i\left[\left(\frac{p_x^2}{2} + I_P + U_P\right)\frac{2\arccos\left(\frac{|p_x|}{A_0}\right)}{\omega} - \frac{3|p_x|}{2\omega}\sqrt{A_0^2 - p_x^2}\right]. \tag{A6}$$

[1] J. D. Jackson, *Classical Electrodynamics*, 3rd ed., (Wiley, New York, 1999).

[2] M. Førre, J. P. Hansen, L. Kocbach, S. Selstø, and L. B. Madsen, Nondipole Ionization Dynamics of Atoms in Superintense High-Frequency Attosecond Pulses, Phys. Rev. Lett. **97**, 043601 (2006).

[3] M. Førre, S. Selstø, J. P. Hansen, T. K. Kjeldsen, and L. B. Madsen, Molecules in intense xuv pulses: Beyond the dipole approximation in linearly and circularly polarized fields, Phys. Rev. A **76**, 033415 (2007).

[4] C. T. L. Smeenk, L. Arissian, B. Zhou, A. Mysyrowicz, D. M. Villeneuve, A. Staudte, and P. B. Corkum, Partitioning of the Linear Photon Momentum in Multiphoton Ionization, Phys. Rev. Lett. **106**, 193002 (2011).

[5] A. S. Titi and G. W. F. Drake, Quantum theory of longitudinal momentum transfer in above-threshold ionization, Phys. Rev. A **85**, 041404(R) (2012).

[6] M. Klaiber, K. Z. Hatsagortsyan, and C. H. Keitel, Above-threshold ionization beyond the dipole approximation, Phys. Rev. A **71**, 033408 (2005).

[7] M. Klaiber, E. Yakaboylu, H. Bauke, K. Z. Hatsagortsyan, and C. H. Keitel, Under-the-Barrier Dynamics in Laser-Induced Relativistic Tunneling, Phys. Rev. Lett. **110**, 153004 (2013).

[8] E. Yakaboylu, M. Klaiber, H. Bauke, K. Z. Hatsagortsyan, and C. H. Keitel, Relativistic features and time delay of laser-induced tunnel ionization, Phys. Rev. A **88**, 063421 (2013).

[9] S. Chelkowski, A. D. Bandrauk, and P. B. Corkum, Photon-momentum transfer in photoionization: From few photons to many, Phys. Rev. A **95**, 053402 (2017).

[10] S. Chelkowski, A. D. Bandrauk, and P. B. Corkum, Photon Momentum Sharing between an Electron and an Ion in Photoionization: From One-Photon (Photoelectric Effect) to Multiphoton Absorption, Phys. Rev. Lett. **113**, 263005 (2014).

[11] S. Chelkowski, A. D. Bandrauk, and P. B. Corkum, Photon-momentum transfer in multiphoton ionization and in time-resolved holography with photoelectrons, Phys. Rev. A **92**, 051401(R) (2015).

[12] A. Ludwig, J. Maurer, B. W. Mayer, C. R. Phillips, L. Gallmann, and U. Keller, Breakdown of the Dipole Approximation in Strong-Field Ionization, Phys. Rev. Lett. **113**, 243001 (2014).

[13] I. A. Ivanov, J. Dubau, and K. T. Kim, Nondipole effects in strong-field ionization, Phys. Rev. A **94**, 033405 (2016).

[14] T. Keil and D. Bauer, Coulomb-corrected strong-field quantum trajectories beyond dipole approximation, J. Phys. B: At., Mol. Opt. Phys. **50**, 194002 (2017).

[15] P.-L. He, D. Lao, and F. He, Strong Field Theories beyond Dipole Approximations in Nonrelativistic Regimes, Phys. Rev. Lett. **118**, 163203 (2017).

[16] J. Daněk, M. Klaiber, K. Z. Hatsagortsyan, C. H. Keitel, B. Willenberg, J. Maurer, B. W. Mayer, C. R. Phillips, L. Gallmann, and U. Keller, Interplay between coulomb-focusing and non-dipole effects in strong-field ionization with elliptical polarization, J. Phys. B: At., Mol. Opt. Phys. **51**, 114001 (2018).

[17] J. Daněk, K. Z. Hatsagortsyan, and C. H. Keitel, Analytical approach to coulomb focusing in strong-field ionization. I. nondipole effects, Phys. Rev. A **97**, 063409 (2018).

[18] B. Böning, W. Paufler, and S. Fritzsche, Nondipole strong-field

approximation for spatially structured laser fields, Phys. Rev. A **99**, 053404 (2019).

[19] M.-X. Wang, H. Liang, X.-R. Xiao, S.-G. Chen, W.-C. Jiang, and L.-Y. Peng, Nondipole effects in atomic dynamic interference, Phys. Rev. A **98**, 023412 (2018).

[20] S. Brenneckeand M. Lein, High-order above-threshold ionization beyond the electric dipole approximation, J. Phys. B: At., Mol. Opt. Phys. **51**, 094005 (2018).

[21] S. Brenneckeand M. Lein, High-order above-threshold ionization beyond the electric dipole approximation: Dependence on the atomic and molecular structure, Phys. Rev. A **98**, 063414 (2018).

[22] S. Brenneckeand M. Lein, Strong-field photoelectron holography beyond the electric dipole approximation: A semiclassical analysis, Phys. Rev. A **100**, 023413 (2019).

[23] B. Willenberg, J. Maurer, U. Keller, J. Daněk, M. Klaiber, N. Teeny, K. Z. Hatsagortsyan, and C. H. Keitel, Holographic interferences in strong-field ionization beyond the dipole approximation: The influence of the peak and focal-volume-averaged laser intensities, Phys. Rev. A **100**, 033417 (2019).

[24] M. Førre and A. S. Simonsen, Generalized velocity-gauge form of the light-matter interaction hamiltonian beyond the dipole approximation, Phys. Rev. A **93**, 013423 (2016).

[25] S. Grundmann, M. Kircher, I. Vela-Perez, G. Nalin, D. Trabert, N. Anders, N. Melzer, J. Rist, A. Pier, N. Strenger, J. Siebert, P. V. Demekhin, L. P. H. Schmidt, F. Trinter, M. S. Schöffler, T. Jahnke, and R. Dörner, Observation of Photoion Backward Emission in Photoionization of He and N_2, Phys. Rev. Lett. **124**, 233201 (2020).

[26] N. Haram, I. Ivanov, H. Xu, K. T. Kim, A. Atia-tul-Noor, U. S. Sainadh, R. D. Glover, D. Chetty, I. V. Litvinyuk, and R. T. Sang, Relativistic Nondipole Effects in Strong-Field Atomic Ionization at Moderate Intensities, Phys. Rev. Lett. **123**, 093201 (2019).

[27] A. Hartung, S. Eckart, S. Brennecke, J. Rist, D. Trabert, K. Fehre, M. Richter, H. Sann, S. Zeller, K. Henrichs, G. Kastirke, J. Hoehl, A. Kalinin, M. S. Schöffler, T. Jahnke, L. P. H. Schmidt, M. Lein, M. Kunitski, and R. Dörner, Magnetic fields alter strong-field ionization, Nat. Phys. **15**, 1222 (2019).

[28] H. Ni, S. Brennecke, X. Gao, P.-L. He, S. Donsa, I. Březinová, F. He, J. Wu, M. Lein, X.-M. Tong, and J. Burgdörfer, Theory of Subcycle Linear Momentum Transfer in Strong-Field Tunneling Ionization, Phys. Rev. Lett. **125**, 073202 (2020).

[29] A. Hartung, S. Brennecke, K. Lin, D. Trabert, K. Fehre, J. Rist, M. S. Schöffler, T. Jahnke, L. P. H. Schmidt, M. Kunitski, M. Lein, R. Dörner, and S. Eckart, Electric Nondipole Effect in Strong-Field Ionization, Phys. Rev. Lett. **126**, 053202 (2021).

[30] S. V. B. Jensen, M. M. Lund, and L. B. Madsen, Nondipole strong-field-approximation hamiltonian, Phys. Rev. A **101**, 043408 (2020).

[31] K. Lin, S. Eckart, A. Hartung, D. Trabert, K. Fehre, J. Rist, L. P. H. Schmidt, M. S. Schöffler, T. Jahnke, M. Kunitski, and R. Dörner, Photoelectron energy peaks shift against the radiation pressure in strong-field ionization, Sci. Adv. **8**, eabn7386 (2022).

[32] K. Lin, S. Brennecke, H. Ni, X. Chen, A. Hartung, D. Trabert, K. Fehre, J. Rist, X.-M. Tong, J. Burgdörfer, L. P. H. Schmidt,

M. S. Schöffler, T. Jahnke, M. Kunitski, F. He, M. Lein, S. Eckart, and R. Dörner, Magnetic-Field Effect in High-Order Above-Threshold Ionization, Phys. Rev. Lett. **128**, 023201 (2022).

[33] R. Kahvedžićand S. Gräfe, Strong-field approximation with leading-order nondipole corrections, Phys. Rev. A **105**, 063102 (2022).

[34] S. Fritzscheand B. Böning, Lorentz-force shifts in strong-field ionization with mid-infrared laser fields, Phys. Rev. Res. **4**, 033031 (2022).

[35] D. B. Miloševićand D. Habibović, Nondipole effects in terahetz-pulse-assisted strong-field ionization, Opt. Express **30**, 29979 (2022).

[36] D. Habibović and D. B. Milošević, Strong-field ionization of atoms beyond the dipole approximation Phys. Rev. A **106**, 033101 (2022).

[37] J. Maurer, B. Willenberg, J. Daněk, B. W. Mayer, C. R. Phillips, L. Gallmann, M. Klaiber, K. Z. Hatsagortsyan, C. H. Keitel, and U. Keller, Probing the ionization wave packet and recollision dynamics with an elliptically polarized strong laser field in the nondipole regime, Phys. Rev. A **97**, 013404 (2018).

[38] M.-X. Wang, S.-G. Chen, H. Liang, and L.-Y. Peng, Review on non-dipole effects in ionization and harmonic generation of atoms and molecules, Chin. Phys. B **29**, 013302 (2020).

[39] N. Haram, R. T. Sang, and I. V. Litvinyuk, Transverse electron momentum distributions in strong-field ionization: nondipole and coulomb focusing effects, J. Phys. B: At., Mol. Opt. Phys. **53**, 154005 (2020).

[40] J. Maurerand U. Keller, Ionization in intense laser fields beyond the electric dipole approximation: concepts, methods, achievements and future directions, J. Phys. B: At., Mol. Opt. Phys. **54**, 094001 (2021).

[41] N. J. Kylstra, R. M. Potvliege, and C. J. Joachain, Photon emission by ions interacting with short intense laser pulses: beyond the dipole approximation, J. Phys. B: At., Mol. Opt. Phys. **34**, L55 (2001).

[42] H. R. Reiss, Relativistic strong-field photoionization, J. Opt. Soc. Am. B **7**, 574 (1990).

[43] H. R. Reiss, Complete keldysh theory and its limiting cases, Phys. Rev. A **42**, 1476 (1990).

[44] G. B. Arfken, H. J. Weber, and F. E. Harris, *Mathematical Methods for Physicists*, 7th ed. (Academic, New York, 2012).

[45] D. B. Milošević, G. G. Paulus, D. Bauer, and W. Becker, Above-threshold ionization by few-cycle pulses, J. Phys. B: At., Mol. Opt. Phys. **39**, R203 (2006).

[46] D. B. Milošević, D. Bauer, and W. Becker, Quantum-orbit theory of high-order atomic processes in intense laser fields, J. Mod. Opt. **53**, 125 (2006).

[47] D. G. Arbó, K. L. Ishikawa, K. Schiessl, E. Persson, and J. Burgdörfer, Intracycle and intercycle interferences in above-threshold ionization: The time grating, Phys. Rev. A **81**, 021403(R) (2010).

[48] D. B. Miloevi and F. Ehlotzky, *Scattering and Reaction Processes in Powerful Laser Fields* (Academic, New York, 2003), pp. 373–532.

[49] H. R. Reiss, Limits on Tunneling Theories of Strong-Field Ionization, Phys. Rev. Lett. **101**, 043002 (2008) [**101**, 159901(E) (2008)].